Nanoscale

PAPER

View Article Online
View Journal | View Issue

Cite this: *Nanoscale*, 2015, **7**, 16737

A dual-stimuli-responsive fluorescent switch ultrathin film†

Zhixiong Li,[a] Ruizheng Liang,[a] Wendi Liu,[a] Dongpeng Yan*[a,b] and Min Wei*[a]

Stimuli-responsive fluorescent switches have shown broad applications in optical devices, biological materials and intelligent responses. Herein, we describe the design and fabrication of a dual-stimuli-responsive fluorescent switch ultrathin film (UTF) *via* a three-step layer-by-layer (LBL) technique: (i) encapsulation of spiropyran (SP) within an amphiphilic block copolymer (PTBEM) to give the (SP@PTBEM) micelle; (ii) the mixture of riboflavin (Rf) and poly(styrene 4-sulfonate) (PSS) to enhance the adhesion ability of small molecules; (iii) assembly of negatively charged SP@PTBEM and Rf–PSS with cationic layered double hydroxide (LDH) nanoplatelets to obtain the $(\text{Rf–PSS/LDH/SP@PTBEM})_n$ UTFs (*n*: bilayer number). The assembly process of the UTFs and their luminescence properties, as monitored by fluorescence spectroscopy and scanning electron microscopy (SEM), present a uniform and ordered layered structure with stepwise growth. The resulting Rf–PSS/LDH/SP@PTBEM UTF serves as a three-state switchable multicolor (green, yellow, and red) luminescent system based on stimulation from UV/Vis light and pH, with an acceptable reversibility. Therefore, this work provides a facile way to fabricate stimuli-responsive solid-state film switches with tunable-color luminescence, which have potential applications in the areas of displays, sensors, and rewritable optical memory and fluorescent logic devices.

Received 8th August 2015,
Accepted 8th September 2015

DOI: 10.1039/c5nr05376e

www.rsc.org/nanoscale

1. Introduction

In the past few decades, there has been growing interest in stimuli-responsive switches and devices due to their broad applications in diverse fields including actuators, catalysis, and detection systems.[1–9] Stimuli-responsive fluorescent switches can undergo significant changes in their structures and photoemission properties under appropriate external stimuli (such as pH, temperature, ionic strength, light, gas, and biomolecules).[10–21] To meet the need for future multifunctional sensing devices, it is highly necessary to fabricate multi-responsive switches which can give sensitive responses to different stimuli simultaneously. Apart from the well-developed single-stimulus-responsive materials, there have been a few examples on bifunctional switchable microgels and nanoparticles responding to different stimuli; for example, by the decoration and linking of UV/pH responsive groups at the molecular scale in the liquid phase, multiple UV/pH fluorescent sensors with multicolor emission can be realized.[22–26] However, the fabrication of bifunctional solid-state films for high-efficiency and portable detection is still limited, since the immobilization process currently suffers from the loss in solid-state emissive intensity (fluorescence quenching) and stability (irreversible photobleaching over time).[27–30] Meanwhile, retaining the property of response to multi-stimuli and avoiding the coupling between different stimulating elements in the solid phase are much difficult compared to that in the liquid phase. Therefore, it is essential to develop new systems and approaches towards bifunctional solid switches based on two or more stimuli.

Recently, inorganic–organic hybrid materials with orderly nanostructures have attracted much attention by taking the advantages of novel functionalities resulted from the non-covalent interactions, which generally differ from those of the pristine materials. Layered double hydroxides (LDHs) are one type of two-dimensional inorganic materials, whose structure can be expressed by the general formula $[\text{M}^{\text{II}}_{1-x}\text{M}^{\text{III}}_x(\text{OH})_2](\text{A}^{n-})_{x/n}\cdot m\text{H}_2\text{O}$ (M^{II} and M^{III} are divalent and trivalent metal ions respectively and A^{n-} is an anion).[31–36] The LDHs have been widely used in catalysis, absorption, imaging and photofunctional materials, by virtue of their tunable chemical composition, layered charge, capability of ion exchange, and good thermal stability.[37–42] Specially, positively-charged LDH

---

[a] *State Key Laboratory of Chemical Resource Engineering, Beijing University of Chemical Technology, Box 98, Beijing 100029, P. R. China. E-mail: yandongpeng001@163.com, weimin@mail.buct.edu.cn; Fax: (+86)10-6442-5385*

[b] *Key Laboratory of Theoretical and Computational Photochemistry, Ministry of Education, College of Chemistry, Beijing Normal University, Beijing 100875, China*

† Electronic supplementary information (ESI) available. See DOI: 10.1039/c5nr05376e

nanosheets or nanoplatelets can be employed to assemble with anionic chromophores and dyes to obtain photofunctional ultrathin films (UTFs).

With the development of multi-stimuli-responsive materials in mind, herein, two representative external stimuli (UV and pH) were chosen as the stimuli-responsive models owing to their extensive applications in intelligent response and detection.[43–47] A bifunctional UV/pH stimuli-responsive UTF switch was fabricated based on the combined assembly of LDH nanoplatelets with spiropyran (SP) and riboflavin (Rf). The design strategy is based on the fact that the SP molecules can respond to UV/visible light with a structural transformation between the closed-ring SP and the open-ring merocyanine (MC) accompanied by a change between non-fluorescence and red-fluorescence.[48–50] Also, the Rf molecule is able to exhibit a pH response, due to the ionization of the imido group that influences the conjugation degree of the isoalloxazine ring and can cause photoluminescence quenching.[51] Therefore, SP and Rf can serve as the independent stimuli-responsive units for the multifunctional switch sensitive to UV/Vis and pH simultaneously. The fabrication of the UTF switch involves three steps by employing the LBL technique (Scheme 1). The as-prepared UTF shows a three-state switchable multicolor fluorescence with sensitive responses to UV/Vis light and pH, which will guarantee the extensive applications of visual detection, intelligent imaging and logic gates. Therefore, the LBL fabrication of UTF gives an alternative and convenient way to obtain a dual-stimuli-responsive solid switch, which is different from the conventional decoration and link synthesis of bifunctional molecules in the liquid phase; the construction method can also be extended to the other stimuli-responsive systems that can provide various changes in color and selectable photoemission.

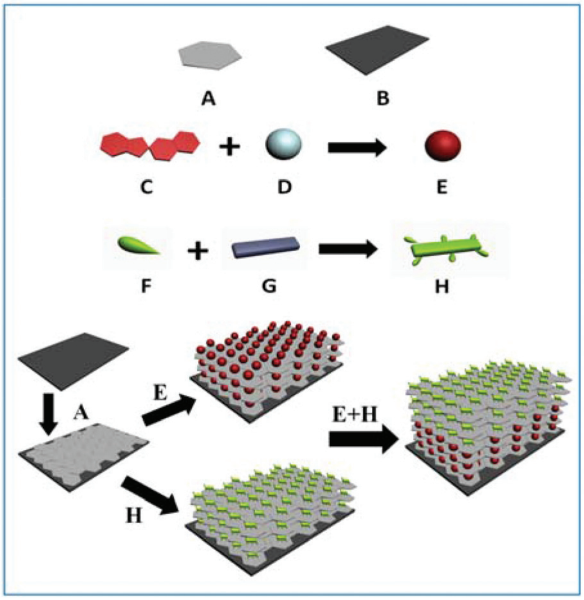

Scheme 1 A schematic representation for the fabrication of multilayered UTFs *via* the LBL self-assembly method: (A) LDH nanoplatelets, (B) quartz glass substrate, (C) SP, (D) PTBEM, (E) SP@PTBEM micelles, (F) Rf, (G) PSS, (H) Rf–PSS hybrid.

2. Experimental section

2.1 Reagents and materials

Poly(*tert*-butyl acrylate-*co*-ethyl acrylate-*co*-methacrylic acid) $[CH_2CH[CO_2C(CH_3)_3]_3]_x[CH_2CH(CO_2C_2H_5)]_y[CH_2C(CH_3)(CO_2H)]_z$ (PTBEM) and polydimethyldiallylammonium chloride (PDDA, M_w = 100 000–200 000) were purchased from Sigma-Aldrich Development Co. Ltd, and poly(styrene sulfonic acid) (PSS, M_w = 70 000) was purchased from J&K Chemical Co. Ltd. 1,3,3-Trimethylindolino-6′-nitrobenzopyrylospiran (spiropyran, M_w = 322.36) was purchased from the Tokyo Chemical Industry. Riboflavin sodium phosphate (riboflavin, Rf, M_w = 478.33) was purchased from Aladdin Reagent. Analytical grade $Mg(NO_3)_2 \cdot 6H_2O$, $Al(NO_3)_3 \cdot 9H_2O$, NaOH and ethylene glycol monobutyl ether ($CH_3(CH_2)_3OCH_2CH_2OH$) were purchased from Beijing Chemical Co. Ltd. All other chemicals were analytical grade and used as received without further purification. Deionized water was used throughout the experimental process.

2.2 Preparation of SP@PTBEM micelle and Rf–PSS hybrid

The SP@PTBEM micelle and Rf–PSS hybrid were synthesized by a liquid synthesis method. The SP was dissolved in the ethylene glycol monobutyl ether (GME) solvent to give a solution (1 mg mL^{-1}); 2 mL of SP in GME solution was added dropwise into a 38 mL of PTBEM micelle solution (0.368 mg mL^{-1}, pH = 7.0, adjusted by 0.1 M NaOH solution) with ultrasonic treatment, keeping the pH value of the final SP@PTBEM micelle at 7.0. The Rf was dissolved in aqueous solution (0.1 mg ml^{-1}), and 5 ml of Rf aqueous solution was added dropwise into a 20 ml of PSS solution (1 mg ml^{-1}) with ultrasonic treatment (20 min) to obtain the Rf–PSS hybrid.

2.3 Preparation of (SP@PTBEM/LDH)$_n$ UTFs, (Rf–PSS/LDH)$_n$ UTFs and (Rf–PSS/LDH/SP@PTBEM)$_n$ UTFs.

The synthesis of MgAl-LDH nanoplatelets was performed according to the separate nucleation and aging step (SNAS) method reported by our group.[52] The quartz substrates were first cleaned in concentrated H_2SO_4/H_2O_2 (30%) (7 : 3, v/v) for 30 min and then washed with pure water. The cleaned substrates were dipped into a PDDA solution (1.0 g L^{-1}) for 20 min, then thoroughly rinsed with water and dried in air, so as to obtain a positively-charged surface. The pretreated substrate was immersed into the negatively-charged SP@PTBEM micelle for 10 min followed by washing and then treated with a colloidal suspension (1 g L^{-1}) of LDH nanoplatelets for another 10 min and washed thoroughly. The multilayered (SP@PTBEM/LDH)$_n$ UTFs were fabricated by the alternate deposition of SP@PTBEM micelles and LDH nanoplatelets for *n* cycles. The fabrication method of (Rf–PSS/LDH)$_n$ multilayered UTFs was similar, except for that the SP@PTBEM micelle was replaced with the Rf–PSS hybrid. The multilayered (Rf–PSS/LDH/SP@PTBEM)$_n$ UTFs were obtained by the alternate deposition of SP@PTBEM micelles, LDH nanoplatelets and Rf–PSS hybrids for n cycles.

2.4 Sample characterization

The fluorescence spectra were recorded on a RF-5301PC fluorospectrophotometer under identical conditions with an excitation wavelength of 365 nm. A Zeiss Supra 55 scanning electron microscope (the accelerating voltage applied was 20 kV) was used to investigate the surface morphology of UTFs. The X-ray photoelectron spectra (XPS) were recorded on a Thermo VGESCALAB 250 X-ray photoelectron spectrometer at a pressure of 2×10^{-9} Pa using Al Kα X-ray as the excitation source. The Commission Internationale de l'Eclairage (CIE) chromaticity color coordinates were recorded by using Konica Minolta CS-2000. The Zeta potential was performed on a Malvern ZEH-3600.

3. Results and discussion

On account of the insolubility and neutrality of SP, the formation of an encapsulation by solvable negatively charged PTBEM (Fig. S1†) is a necessary and effective step. The SP@PTBEM micelles ensure the hydrophobic terminal combining with SP, while the hydrophilic terminal with the negative charge is attached to LDH nanoplatelets for the construction of UTFs.[53] Then, we made a comparison study between the negative electricity of Rf and Rf–PSS hybrids. Fig. S2† shows a weak negative electricity of Rf (Zeta potential: −21.5 mV); while Fig. S3† displays an obvious enhancement in the negative electricity after hybridization of Rf and PSS (Zeta potential: −36.0 mV). This is beneficial to impose a strong electrostatic interaction with the positively-charged LDH nanosheets (Fig. S4†: Zeta potential: +27.0 mV). The (SP@PTBEM/LDH)$_n$ and (Rf–PSS/LDH)$_n$ UTFs can be constructed by assembling the LDH nanoplatelets with SP@PTBEM micelles and Rf–PSS hybrids respectively. The heterogeneous (Rf–PSS/LDH/SP@PTBEM)$_n$ UTF was prepared by assembling the LDH nanoplatelets with SP@PTBEM micelles and Rf–PSS hybrids alternately. Scheme 1 shows the detailed assembly process of the multilayered UTF systems.

3.1 Fabrication of (SP@PTBEM/LDH)$_n$ and (Rf–PSS/LDH)$_n$ UTFs

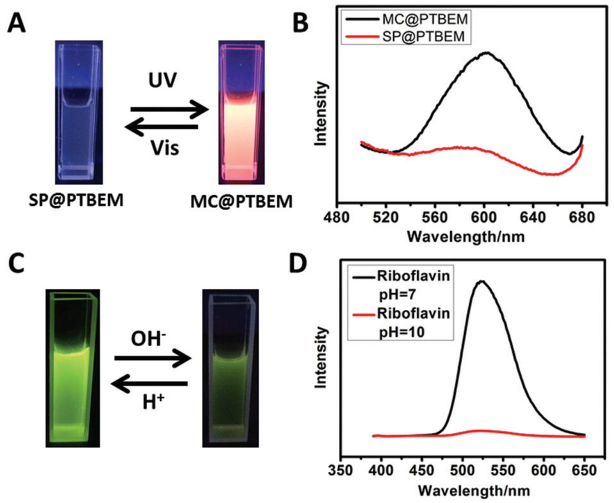

Fig. 1 (A) Reversible fluorescence transformation between SP@PTBEM and MC@PTBEM triggered by UV and visible light. (B) The photoluminescence spectra of SP@PTBEM and MC@PTBEM solutions. (C) Fluorescence photographs under UV light (365 nm) and (D) photoluminescence spectra of Rf–PSS's reversible response to pH between 7 and 10.

The SP molecule undergoes a structural transformation from a non-fluorescence closed-ring state to red-fluorescent open-ring MC upon triggering by UV light, and subsequently reverts back to SP by visible light.[27,54,55] In this work, the amphiphilic and negative copolymer PTBEM was employed to enhance the fluorescence of MC by localization of the fluorophores in the hydrophobic environment of vesicles (Fig. S5†),[27,56,57] which is particularly important in the development of switchable fluorescent devices. The reversible transformation from SP@PTBEM to MC@PTBEM with a distinct fluorescence change can be observed with the naked eye (Fig. 1A and B), and the relevant UV-Vis absorption spectra are shown in Fig. S6.†

Rf, well-known as vitamin B$_2$, plays a central role in biological systems as a redox-active unit of cofactors.[58] In addition, the isoalloxazine moiety of Rf is fluorescence active and the chiral ribityl group makes it soluble in water.[59] The imido protons of Rf are labile at high pH of the medium and can quench the fluorescence of Rf.[51] Here, a mixture of Rf and PSS shows a strong green-fluorescence at pH = 7 and a weak fluorescence at pH = 10, (Fig. 1C and D), and the relevant UV-Vis absorption spectra are shown in Fig. S7.† Therefore, the Rf–PSS hybrid has a potential for responding to alkaline gas (such as NH_3) that can lead to the change in pH.

The (Rf–PSS/LDH)$_n$ UTFs were firstly fabricated by assembling the Rf–PSS hybrid with LDH nanoplatelets onto the quartz substrate *via* the LBL deposition technique. The fluorescence spectra show an emission at 525–535 nm for these UTFs (Fig. 2A and C), and the slight red-shift with the growth of n may be assigned to the partial aggregation of Rf, similar to its solution state (Fig. S8 and S9†). The (SP@PTBEM/LDH)$_n$ UTFs were subsequently fabricated by assembling SP@PTBEM micelles with LDH nanoplatelets showing the fluorescence emission at 610 nm (Fig. 2B and D†). Two kinds of UTFs show bright fluorescence display and the intensity enhances linearly along with the increase in bilayer number, which is an extremely important criteria in practical applications of visual stimuli-responsive switches. Based on the change of fluorescence intensity *versus* n, the (SP@PTBEM/LDH)$_{20}$ and (Rf–PSS/LDH)$_{20}$ UTFs were chosen for further study.

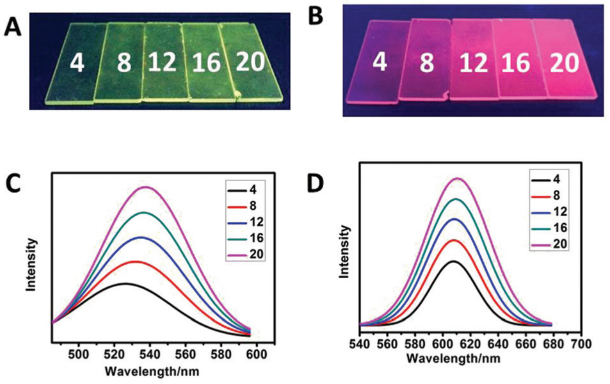

Fig. 2 Photographs of (A) (Rf–PSS/LDH)$_n$ and (B) (SP@PTBEM/LDH)$_n$ UTFs under 365 nm UV illumination. (C, D) Photoemission spectra of (Rf–PSS/LDH)$_n$ and (SP@PTBEM/LDH)$_n$ UTFs from n = 4 to 20, respectively.

3.2 Structural and morphological characterization

The surface morphology of (SP@PTBEM/LDH)$_{20}$ and (Rf–PSS/LDH)$_{20}$ UTFs was investigated by SEM. The SEM image and XRD pattern of LDH nanoplatelets show a hexagonal platelet shape and an average diameter of 50–100 nm (Fig. S10 and S11†). The SP@PTBEM micelle is revealed as an individual spherical morphology with a uniform diameter of ~100 nm (Fig. 3A). The top-view of the Rf–PSS hybrid is shown in Fig. 3B, and a sticky colloidal interface linker can be observed, which is beneficial to the assembly with LDH nanoplatelets.

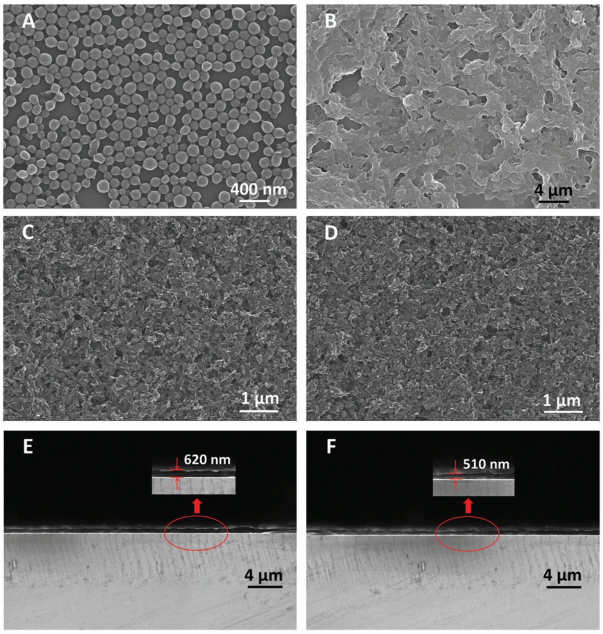

Fig. 3 SEM images of (A) SP@PTBEM micelles and (B) Rf–PSS hybrid; top-view SEM image of (C) (SP@PTBEM/LDH)$_{20}$ and (D) (Rf–PSS/LDH)$_{20}$ UTFs with LDH nanoplatelets as the terminal layer; side-view SEM images of (E) (SP@PTBEM/LDH)$_{20}$ and (F) (Rf–PSS/LDH)$_{20}$ UTFs.

Fig. 3C and D display the surface of (Rf–PSS/LDH)$_{20}$ and (SP@PTBEM/LDH)$_{20}$ UTFs with the LDH nanoplatelets as the terminal layer respectively, from which a relatively uniform and smooth surface can be observed. The side-view SEM images (Fig. 3E and F) give an estimation on the thickness of (SP@PTBEM/LDH)$_{20}$ and (Rf–PSS/LDH)$_{20}$ UTFs, which shows an approximately linear increase in film thickness as a function of n, with a bilayer thickness of 31 nm and 25 nm for (SP@PTBEM/LDH)$_{20}$ and (Rf–PSS/LDH)$_{20}$ UTFs respectively (Fig. S12 and S13†).

3.3 Stimuli-responsive behavior of Rf–PSS/LDH/SP@PTBEM UTFs

As an idealized dual-stimuli-responsive switch, the independence of each response to external stimulus is very important. In this work, the switch is expected to respond to UV and NH_3 simultaneously, and the coupling between each stimulus needs to be avoided. Two control experiments were made firstly: when the (Rf–PSS/LDH)$_{20}$ and (SP@PTBEM/LDH)$_{20}$ UTFs were treated under an alkaline atmosphere, it was observed that the intensity at 525 nm of the (Rf–PSS/LDH)$_{20}$ UTF declines gradually with time (Fig. 4A). While, the intensity at 610 nm of the (SP@PTBEM/LDH)$_{20}$ UTF was almost unaltered (Fig. 4B), which confirmed the specific response to pH for Rf–PSS/LDHs. Additionally, upon irradiation of (Rf–PSS/LDH)$_{20}$ and (SP@PTBEM/LDH)$_{20}$ UTFs by UV light, the intensity of (Rf–PSS/LDHs)$_{20}$ remained invariable, while that of the (SP@PTBEM/LDHs)$_{20}$ enhanced obviously (Fig. 4C and D), demonstrating the specific response to UV light for SP@PTBEM/LDHs. These observations guarantee the particular responses to NH_3 and UV for Rf–PSS/LDH and SP@PTBEM/LDH units respectively.

The variation mechanism from SP to MC can be understood by the detection of the change in binding energy of the N 1s core level region. Based on the X-ray photoemission spectrum

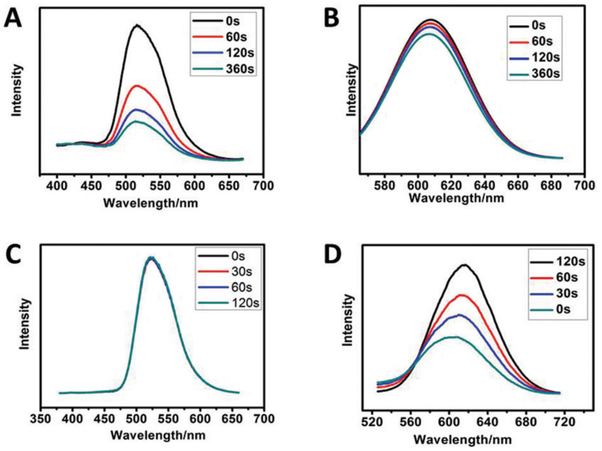

Fig. 4 Photoemission spectra of (A) (Rf–PSS/LDH)$_{20}$ and (B) (SP@PTBEM/LDH)$_{20}$ UTFs under an alkaline atmosphere. Photoemission spectra of (C) (Rf–PSS/LDH)$_{20}$ and (D) (SP@PTBEM/LDH)$_{20}$ UTFs irradiated by UV light for 120 s.

(XPS), the binding energy of N 1s for SP (indoline nitrogen) and MC (N^+ species) is located at about 400 eV and 401.3 eV, respectively, which offers an effective indication of these two species.[60] For the SP@PTBEM without UV illumination, the peak at 400 eV is observed (Fig. S14A†), revealing the existence of SP. After UV irradiation at 365 nm for 120 s, the N 1s peak at 400 eV becomes unpronounced while the peak at 401.3 eV increases largely (Fig. S14B†), demonstrating that the SP molecules in the micelle transform to MC upon UV irradiation.[61] The same measure was also used for the Rf molecule. According to the previous study,[62] the change in the pH value leads to an interesting transformation of the Rf molecular structure: the labile proton of the imido group becomes ionized under basic conditions (Fig. S15†). Therefore, the response of Rf to pH can also be illuminated by XPS. For Rf–PSS at pH = 7, the peaks of the N 1s core level region at 399.8 eV and 402.4 eV are observed (Fig. 5A), which represent the conjugated N (C=N type) and imido group respectively.[63,64] For Rf–PSS at pH = 10, the peak at 402.4 eV disappears and only the peak at 399.8 eV is observed (Fig. 5B), revealing that the labile proton of the imido group becomes ionized which can hamper the conjugation of the isoalloxazine ring and result in the photoluminescence quenching.[51]

Reversibility is an extremely important criterion in practical applications of stimuli-responsive switches or optoelectronic devices. In this work, the $(Rf–PSS/LDH)_{20}$ and $(SP@PTBEM/LDH)_{20}$ UTFs display good reversibility, which are accompanied by a remarkable change in the emission color. Green-fluorescence of the $(Rf–PSS/LDH)_{20}$ UTF turns to non-fluorescence upon stimulation by alkaline gas (NH_3), which can return to the initial state by soaking in H_2O (Fig. 6A top). The $(SP@PTBEM/LDH)_{20}$ UTF changes from red-fluorescence to non-fluorescence by alternative Vis/UV light irradiation (Fig. 6A down). The fluorescence reversibility of the two types of UTFs can be recycled at least five times (Fig. 6B).

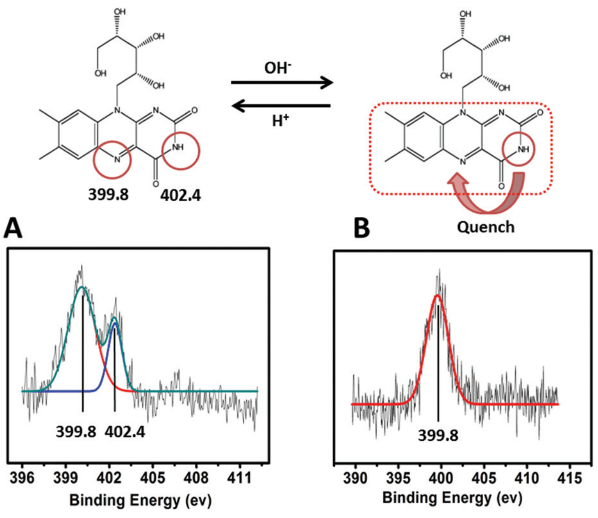

Fig. 5 X-ray photoemission spectra of the N 1s core level regions of Rf–PSS when the pH values are 7 (A) and 10 (B) respectively.

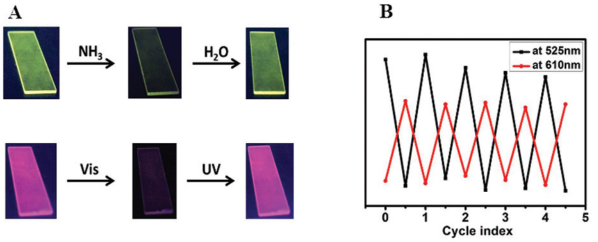

Fig. 6 (A) The photographs of reversibility by alternative stimulation with NH_3 and H_2O for $(Rf–PSS/LDH)_{20}$, and the reversibility by alternative Vis/UV light irradiation for $(SP@PTBEM/LDHs)_{20}$. (B) The intensity reversibility recorded for $(Rf–PSS/LDH)_{20}$ and $(SP@PTBEM/LDHs)_{20}$ at 525 nm and 610 nm respectively.

Based on the single-stimulus-responsive fluorescence detected above, the dual-stimuli-responsive $(Rf–PSS/LDH/SP@PTBEM)_{20}$ UTF switch was further fabricated. The schematic colorful change of the UTF is shown in Fig. 7A, and Fig. 7B displays the corresponding photoemission spectra of the three states. The original fluorescence color of UTF shows green fluorescence belonging to Rf only. When the single stimulation of UV is imported, SP turns into the MC state with red-fluorescence; the UTF displays a yellow-emission color because of a mixed component of red emission (MC) and green emission (Rf). Moreover, the UTF displays a red-fluorescence under the stimulation of both UV and NH_3, because the fluorescence of Rf has been quenched by NH_3, and the emission is provided by MC only. The reversible three-state switchable multicolor luminescent system based on the $(Rf–PSS/LDH/SP@PTBEM)_{20}$ UTF is displayed in Fig. 7C, and the switch can be induced reversibly by UV/Vis and NH_3/H_2O treatments.

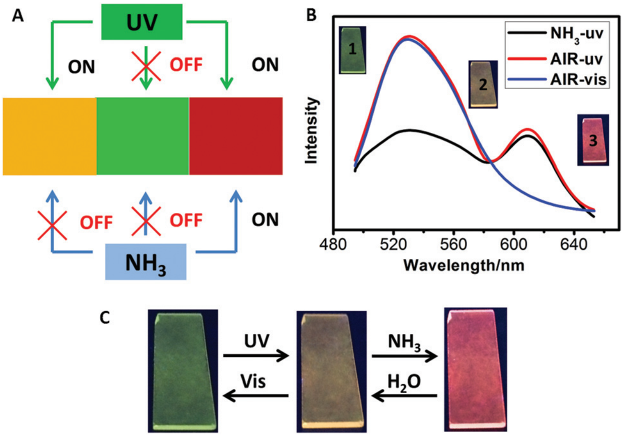

Fig. 7 (A) Schematic representation for UV and NH_3 stimuli-responses of the $(Rf–PSS/LDH/SP@PTBEM)_{20}$ UTF. (B) Photoemission spectra of the $(Rf–PSS/LDH/SP@PTBEM)_{20}$ UTF at the three states; the inset shows the photographs of three-state UTFs under 365 nm UV illumination. (C) Reversible three-state switchable multicolor luminescent system based on the $(Rf–PSS/LDH/SP@PTBEM)_{20}$ UTF.

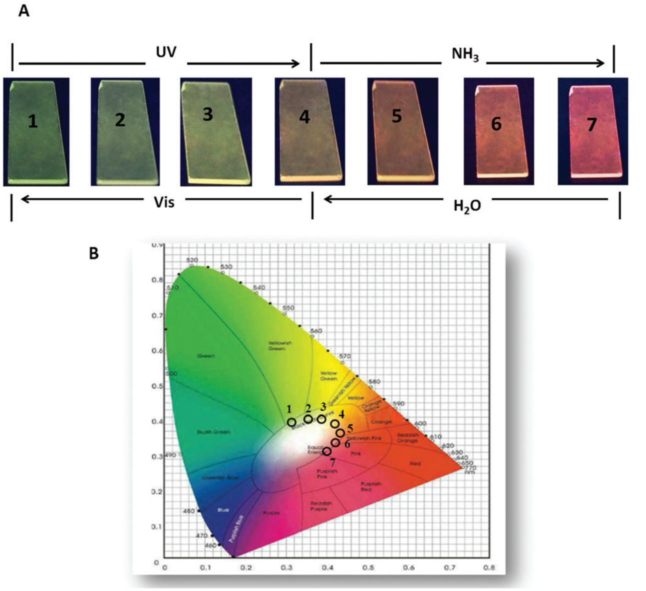

Fig. 8 (A) Continuous variable photographs of the (Rf–PSS/LDH/SP@PTBEM)$_{20}$ UTF by stimulating with UV/Vis (1–4) and NH_3/H_2O (4–7). (B) The corresponding variation in the color coordinates of the (Rf–PSS/LDH/SP@PTBEM)$_{20}$ UTF with the stimulation of UV/Vis and NH_3/H_2O.

The continuous and reversible stimuli-responsive variation of the (Rf–PSS/LDH/SP@PTBEM)$_{20}$ UTF is shown in Fig. 8A, and the original UTF (no. 1) is green-fluorescence. The UTF (no. 1–4) moves gradually closer to yellow-fluorescence during irradiation by UV, and reaches the final state (no. 4) after 120 s. Subsequently, the UTF (no. 4–7) turns to red-fluorescence with the stimulation of NH_3. In addition, the UTF can be recovered with the aid of visible light and H_2O. Therefore, a multi-stimuli-responsive and time-dependent dynamic fluorescent switch based on the (Rf–PSS/LDH/SP@PTBEM)$_{20}$ UTF has been fabricated, which responds to UV and pH (including the alkali gas such as NH_3) with a three-state fluorescence reversibility, and the corresponding variation in the color coordinates with the stimulation of UV/Vis and NH_3/H_2O has been shown in Fig. 8B.

4. Conclusion

In conclusion, a dual-stimuli-responsive switch film was designed and fabricated based on the units of Rf–PSS hybrids, SP@PTBEM micelles and LDH nanoplatelets *via* a two-step self-assembly. The UTFs exhibit a periodic long-range stacking orderly structure and controllable photoemission intensity. The luminescent color of the resulting hybrid UTF can be easily tuned between the three states by alternative UV/Vis and NH_3/H_2O treatments. Compared with the previously reported studies, the layer-by-layer assembly method in this work gives an alternative and convenient way to obtain a dual-stimuli-responsive solid-state switch, which is different from the conventional decoration and link synthesis of bifunctional molecules in the liquid phase and other single-stimuli-responsive systems. Moreover, the reversible three-state multicolor fluorescence (red, yellow and green) with time-dependent emission also facilitates the construction of fluorescence-based logic gates and sensors. It is anticipated that the strategy demonstrated in this work can be extended to the fabrication of other multi-responsive film switches with unique functionality, which would facilitate their potential applications in displays, sensors, and rewritable optical memory and fluorescent logic devices.

Acknowledgements

This work was supported by the 973 Program (Grant No. 2014CB932104), the National Natural Science Foundation of China (NSFC), the Scientific Fund from Beijing Municipal Commission of Education, and the Beijing Municipal Natural Science Foundation (Grant No. 2152016). M.W. appreciates the China National Funds for Distinguished Young Scholars of the NSFC.

Notes and references

1 J. Kim, S. Nayak and L. A. Lyon, *J. Am. Chem. Soc.*, 2005, **127**, 9588–9592.
2 M. J. Serpe, J. Kim and L. A. Lyon, *Adv. Mater.*, 2004, **16**, 184–187.
3 S. Nayak and L. A. Lyon, *Angew. Chem., Int. Ed.*, 2004, **43**, 6706–6709.
4 I. Tokarev and S. Minko, *Adv. Mater.*, 2010, **22**, 3446–3462.
5 M. Motornov, Y. Roiter, I. Tokarev and S. Minko, *Prog. Polym. Sci.*, 2010, **35**, 174–211.
6 M. R. Molla, P. Rangadurai, G. M. Pavan and S. Thayumanavan, *Nanoscale*, 2015, **7**, 3817–3837.
7 S. Chen, Y. Ruan, J. D. Brown, J. Gallucci, V. Maslak, C. M. Hadad and J. D. Badjic, *J. Am. Chem. Soc.*, 2013, **135**, 14964–14967.
8 K. S. Soppimath, D. C. Tian and Y. Yang, *Adv. Mater.*, 2005, **17**, 318–323.
9 D. Wang, T. Liu, J. Yin and S. Liu, *Macromolecules*, 2011, **44**, 2282–2290.
10 W. Shi, S. He, M. Wei, D. G. Evans and X. Duan, *Adv. Funct. Mater.*, 2010, **20**, 3856–3863.
11 M. Lee, S. Lee and L. Jiang, *J. Am. Chem. Soc.*, 2004, **126**, 12724–12725.
12 E. R. Gillies, T. B. Jonsson and J. M. J. Fréchet, *J. Am. Chem. Soc.*, 2004, **126**, 11936–11943.
13 X. Yana and X. An, *Nanoscale*, 2013, **5**, 6280–6283.
14 J. Hu, G. Zhang, Y. Geng and S. Liu, *Macromolecules*, 2011, **44**, 8207–8214.
15 V. Fasano, M. Baroncini, M. Moffa, D. Iandolo, A. Camposeo, A. Credi and D. Pisignano, *J. Am. Chem. Soc.*, 2014, **136**, 14245–14254.
16 J. Borges, L. C. Rodrigues, R. L. Reis and J. F. Mano, *Adv. Funct. Mater.*, 2014, **24**, 5624–5648.

17 H. Iida, S. Iwahana, T. Mizoguchi and E. Yashima, *J. Am. Chem. Soc.*, 2012, **134**, 15103–15113.

18 Z. Li, J. Lu, S. Li, S. Qin and Y. Qin, *Adv. Mater.*, 2012, **24**, 6053–6057.

19 Y. Wang, M. S. Shim, N. S. Levinson, H. W. Sung and Y. Xia, *Adv. Funct. Mater.*, 2014, **24**, 4206–4220.

20 M. S. Shim, C. S. Kim, Y. Ahn, Z. Chen and Y. J. Kwon, *J. Am. Chem. Soc.*, 2010, **132**, 8316–8324.

21 Q. Liu, J. Peng, L. Sun and F. Li, *ACS Nano*, 2011, **5**, 8040–8048.

22 C. Li, Y. Zhang, J. Hu, J. Cheng and S. Liu, *Angew. Chem., Int. Ed.*, 2010, **49**, 5120–5124.

23 J. Yin, H. Hu, Y. Wu and S. Liu, *Polym. Chem.*, 2011, **2**, 363–371.

24 C. Li and S. Liu, *J. Mater. Chem.*, 2010, **20**, 10716–10723.

25 K. Matsubara, M. Watanabe and Y. Takeoka, *Angew. Chem., Int. Ed.*, 2007, **46**, 1688–1692.

26 S. Das, P. Ranjan, P. S. Maiti, G. Singh, G. Leitus and R. Klajn, *Adv. Mater.*, 2013, **25**, 422–426.

27 R. Klajn, *Chem. Rev.*, 2014, **43**, 148–184.

28 L. Florea, A. McKeon, D. Diamond and F. Benito-Lopez, *Langmuir*, 2013, **29**, 2790–2797.

29 B. Kuswandi and R. Narayanaswamy, *J. Anal. Chem.*, 1999, **364**, 605–607.

30 F. Buchholz, N. Buschmann and K. Cammann, *Sens. Actuators, B*, 1992, **9**, 41–47.

31 Q. Wang and D. O'Hare, *Chem. Rev.*, 2012, **112**, 4124–4155.

32 G. R. Williams and D. O'Hare, *J. Mater. Chem.*, 2006, **16**, 3065–3074.

33 A. M. Fogg, A. J. Freij and G. M. Parkinson, *Chem. Mater.*, 2002, **14**, 232–234.

34 F. Leroux and C. Taviot-Guého, *J. Mater. Chem.*, 2005, **15**, 3628–3642.

35 L. Li, R. Ma, Y. Ebina, N. Iyi and T. Sasaki, *Chem. Mater.*, 2005, **17**, 4386–4391.

36 Z. Liu, R. Ma, M. Osada, N. Iyi, Y. Ebina, K. Takada and T. Sasaki, *J. Am. Chem. Soc.*, 2006, **128**, 4872–4880.

37 Y. Zhao, B. Li, Q. Wang, W. Gao, C. J. Wang, M. Wei, D. G. Evans, X. Duan and D. O'Hare, *Chem. Sci.*, 2014, **5**, 951–958.

38 Y. Dou, S. Zhang, T. Pan, S. Xu, A. Zhou, M. Pu, H. Yan, J. Han, M. Wei, D. G. Evans and X. Duan, *Adv. Funct. Mater.*, 2015, **25**, 2243–2249.

39 R. Liang, S. Xu, D. Yan, W. Shi, R. Tian, H. Yan, M. Wei, D. G. Evans and X. Duan, *Adv. Funct. Mater.*, 2012, **22**, 4940–4948.

40 R. Tian, R. Liang, D. Yan, W. Shi, X. Yu, M. Wei, L. S. Li, D. G. Evans and X. Duan, *J. Mater. Chem. C*, 2013, **1**, 5654–5660.

41 D. Yan, J. Lu, J. Ma, M. Wei, D. G. Evans and X. Duan, *Angew. Chem., Int. Ed.*, 2011, **50**, 720–723.

42 D. Yan, J. Lu, M. Wei, J. Han, J. Ma, F. Li, D. G. Evans and X. Duan, *Angew. Chem., Int. Ed.*, 2009, **48**, 3073–3076.

43 N. Fomina, C. McFearin, M. Sermsakdi, O. Edigin and A. Almutairi, *J. Am. Chem. Soc.*, 2010, **132**, 9540–9542.

44 D. Tarn, D. P. Ferris, J. C. Barnes, M. W. Ambrogio, J. F. Stoddartb and J. I. Zink, *Nanoscale*, 2014, **6**, 3335–3343.

45 K. Zhou, H. Liu, S. Zhang, X. Huang, Y. Wang, G. Huang, B. D. Sumer and J. Gao, *J. Am. Chem. Soc.*, 2012, **134**, 7803–7811.

46 X. Wu, Z. Wang, D. Zhu, S. Zong, L. Yang, Y. Zhong and Y. Cui, *ACS Appl. Mater. Interfaces*, 2013, **5**, 10895–10903.

47 Z. Xu, S. Liu, Y. Kang and M. Wang, *Nanoscale*, 2015, **7**, 5859–5868.

48 Z. Li, S. Wan, W. Shi, M. Wei, M. Yin, W. Yang, D. G. Evans and X. Duan, *J. Phys. Chem. C*, 2015, **119**, 7428–7435.

49 M. Zhu, G. Zhang, C. Li, M. P. Aldred, E. Chang, R. A. Drezek and A. D. Q. Li, *J. Am. Chem. Soc.*, 2011, **133**, 365–372.

50 L. Zhu, M. Zhu, J. K. Hurst and A. D. Q. Li, *J. Am. Chem. Soc.*, 2005, **127**, 8968–8970.

51 A. Saha, S. Manna and A. K. Nandi, *Soft Matter*, 2009, **5**, 3992–3996.

52 R. P. Bontchev, S. Liu, J. L. Krumhansl, J. Voigt and T. M. Nenoff, *Chem. Mater.*, 2003, **15**, 3669–3675.

53 S. Li, J. Lu, H. Ma, D. Yan, Z. Li, S. Qin, D. G. Evans and X. Duan, *J. Phys. Chem. C*, 2012, **116**, 12836–12843.

54 H. Tian and Y. Feng, *J. Mater. Chem.*, 2008, **18**, 1617–1622.

55 W. Fuss, C. Kosmidis, W. E. Schmid and S. A. Trushin, *Angew. Chem., Int. Ed.*, 2004, **43**, 4178–4182.

56 C. Huang, Y. Wang, C. Hong and C. Pan, *Macromol. Rapid Commun.*, 2011, **32**, 1174–1179.

57 Y. H. Chan, M. E. Gallina, X. Zhang, I. C. Wu, Y. Jin, W. Sun and D. T. Chiu, *Anal. Chem.*, 2012, **84**, 9431–9438.

58 G. R. Penzer and G. K. Radda, *Q. Rev., Chem. Soc.*, 1967, **21**, 43–65.

59 L. Li, *Macromolecules*, 2002, **35**, 5990–5998.

60 E. Pigois, D. Gayot, M. Delamar, M. Leclerc and M. M. Chehimi, *Relat. Phenom.*, 1990, **53**, 79–86.

61 O. Ivashenko, J. T. van Herpt, B. L. Feringa, P. Rudolf and W. R. Browne, *Langmuir*, 2013, **29**, 4290–4297.

62 G. R. Penzer and G. K. Radda, *Q. Rev., Chem. Soc.*, 1967, **21**, 43–65.

63 Y. Wu, S. Fang and Y. Jiang, *Solid State Ionics*, 1999, **120**, 117–123.

64 H. Schmiersa, J. Friebela, P. Streubelb, R. Hesseb and R. Köpsela, *Carbon*, 1999, **37**, 1965–1978.